Symmetric and Asymmetric Push-Pull Conjugates: Significance of Pull Group Strength on Charge Transfer and Separation

Youngwoo Jang,[†] Yogajivan Rout,[‡] Rajneesh Misra[*,‡] and Francis D'Souza[*,†]

[†]Department of Chemistry, University of North Texas, 1155 Union Circle, #305070, Denton, TX 76203-5017, USA

[‡]Department of Chemistry, Indian Institute of Technology, Indore 453552, India.

ABSTRACT: The effect of acceptor strength on excited state charge-transfer (CT) and charge separation (CS) in central phenothiazine (PTZ) derived symmetric **1** (PTZ-(TCBD-TPA)$_2$) and asymmetric, **2** (PTZ-(TCBD/DCNQ-TPA)$_2$) push-pull conjugates, in which triphenylamine (TPA) act as end capping and 1,1,4,4–tetracyanobuta–1,3–diene (TCBD) and cyclohexa–2,5–diene–1,4–ylidene–expanded TCBD (DCNQ) act as electron acceptor units is reported. Due to strong push-pull effects, intramolecular charge transfer (ICT) was observed in the ground state extending the absorption into the near-IR region. Electrochemical, spectroelectrochemical and computational studies coupled with energy level calculations predicted both **1** and **2** to be efficient candidates for ultrafast charge transfer. Subsequent femtosecond transient absorption studies along with global target analysis, performed in both polar and nonpolar solvents, confirmed such processes in which the CS was efficient in asymmetric **2** having both TCBD and DCNQ acceptors in polar benzonitrile while in toluene, only charge transfer was witnessed. This work highlights significance of number and strength of electron acceptor entities and the role of solvent polarity in multi-modular push-push systems to achieve ultrafast CS.

KEYWORDS Intramolecular charge transfer, ultrafast charge separation, symmetric and asymmetric multi-modular push-pull systems.

INTRODUCTION

Multi-modular push-pull systems comprised of various heterocyclic units have gained considerable interest of the scientific community in recent years due to their excellent performance in organic light emitting diodes (OLEDs),[1-3] non-linear optics (NLO)[4-5] and organic photovoltaics (OPVs).[6-7] Our groups have been particularly interested in the design and photophysical characterization of heterocyclic π-conjugated push-pull systems for such applications.[8-16] In the design of push-pull systems, phenothiazine is often used as an electron donor unit due to the presence of electron-rich sulfur and nitrogen atoms in the heterocyclic ring, also exhibiting nonplanar geometry with good thermal and electrochemical stability.[17-19] Due to these excellent properties, they have been employed to build a variety of donor and acceptor substituted symmetrical and asymmetrical derivatives in which phenothiazine acts as a central unit.[20-27] A literature survey shows that both symmetrical and asymmetrical phenothiazine derivatives have been used as materials for organic photovoltaics.[17-27] Although much progress have been made on the syntheses front, ultrafast spectroscopic studies on such push-pull systems with phenothiazine central core are still limited,[28-29] thus limiting their usage in the envisioned applications. To overcome this limitation, recently we designed symmetrical and asymmetrical push-pull phenothiazine chromophores by incorporating TCBD and DCNQ into a central PTZ and terminal TPA derived molecular system, **C2**. The symmetric compound **1**, possess two TPA-TCBD entities on the central PTZ while the asymmetric compound **2** possess one TPA-TCBD and another TPA-DCNQ units on the central PTZ (see Figure 1).[30] In our synthetic strategy, powerful electron acceptors such as tetracyanobutadiene (TCBD) and cyclohexa–2,5–diene–1,4–ylidene–expanded TCBD (DCNQ) were introduced by [2+2] cycloaddition–retroelectrocyclization reaction into PTZ molecular farework.[31-34] As demonstrated here, strong ground and excited state CT has been witnessed in these systems, especially in the asymmetric **2**. Further, fs-TA coupled with global target analysis of spectral data revealed ultrafast CT and CS both in polar benzonitrile and only CT in nonpolar toluene. The significance of asymmetric functionalization in improving photophysical properties is borne out in the present study.

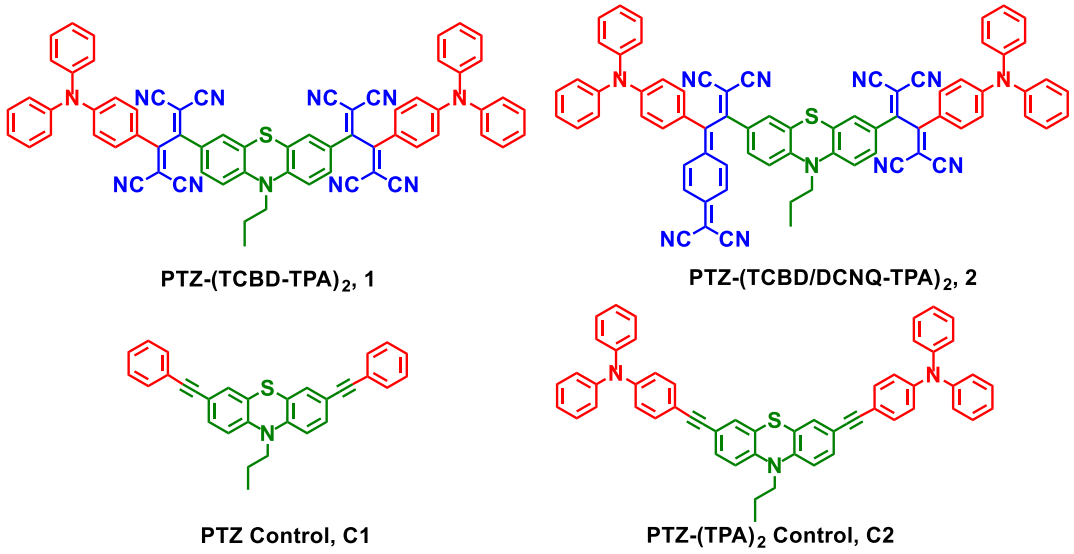

Figure 1. Structures of the symmetric (**1**) and asymmetric (**2**) push-pull systems and the control compounds (**C1** and **C2**) investigated here.

EXPERIMENTAL SECTION

General methods

The UV-visible spectral measurements were carried out with a Shimadzu Model 2550 double monochromator UV-visible spectrophotometer. The fluorescence emission was monitored by using a Horiba Yvon Nanolog coupled with time-correlated single photon counting with nanoLED excitation sources. A right angle detection method was used. Differential pulse and cyclic voltammograms were recorded on an EG&G PARSTAT electrochemical analyzer using a three electrode system. A platinum button electrode was used as the working electrode. A platinum wire served as the counter electrode and an Ag/AgCl electrode was used as the reference electrode. Ferrocene/ferrocenium redox couple was used as an internal standard. All the solutions were purged prior to electrochemical and spectral measurements using argon gas.

Femtosecond transient absorption spectroscopy experiments were performed using an ultrafast femtosecond laser source (Libra) by Coherent incorporating a diode-pumped, modelocked Ti:sapphire laser (Vitesse) and a diode-pumped intracavity doubled Nd:YLF laser (Evolution) to generate a compressed laser output of 1.45 W. For optical detection, a Helios transient absorption spectrometer coupled with a femtosecond harmonics generator, both provided by Ultrafast

Systems LLC, was used. The sources for the pump and probe pulses were derived from the fundamental output of Libra (Compressed output 1.45 W, pulse width 100 fs) at a repetition rate of 1 kHz; 95% of the fundamental output of the laser was introduced into a TOPAS-Prime-OPA system with a 290−2600 nm tuning range from Altos Photonics Inc., (Bozeman, MT), while the rest of the output was used for generation of a white light continuum. Kinetic traces at appropriate wavelengths were assembled from the time-resolved spectral data. Data analysis was performed using Surface Xplorer software supplied by Ultrafast Systems. All measurements were conducted in degassed solutions at 298 K. The estimated error in the reported rate constants is ±10%.

Synthesis and characterization of the studied multi-modular push-pull conjugates and their control compounds is given elsewhere.[30,35] Prior performing spectral and photochemical studies, the compounds were purified over column chromatography and the purity was check by thin-layer chromatography.

RESULTS AND DISCUSSION

Figure 2a shows the absorption spectra of compounds **1** and **2** along with the control compounds, **C1** and **C2** in benzonitrile. The phenyl acetylene functionalized PTZ in **C1** revealed a single absorption band at 375 nm. For **C2**, having two terminal TPA entities, two peaks at 351 and 387 nm were observed. Introduction of two TCBD electron acceptors in **1** further red-shifted the absorption into the visible region with a peak maxima at 490 nm coupled with a relatively narrow shoulder peak at 435 nm. This feature was especially clear in toluene (see Figure S1 in SI). Interestingly, incorporation of TCBD and DCNQ entities on either side of PTZ in **2** resulted further red-shift and splitting of the visible bands. The first peak was located at 480 nm while the second one was at 634 nm. By comparison with compounds reported earlier,[8] the high-energy peak was attributed to π−π transition (locally excited, LE) and the low-energy peak to the ICT transitions. Imporantly, the spectrum of **2** covered a wide 300-850 nm range revealing its panchromatic performance.

Both **C1** and **C2** were found to be fluorescent with peak maxima located at 488 nm for **C1** and 492 nm for **C2** (Figure 2b). Fluorescence lifetimes measured from time correlated single photon counting (TCSPC) method resulted in a lifetime of 5.14 ns for **C1** and 2.72 ns for **C2** (see Figure 2b inset for decay curves). Very weak emission, centered around 560 nm for **1** and 700 nm for **2** (overlapped with the Solvent Raman peaks) was observed (see Figure S2 in SI) upon

excitation corresponding to CT peak maxima revealing presence of very weak CT emission in these compounds. The absorption and fluorescence trend in nonpolar toluene were almost the same (Figure S1a and b). Only compounds **C1** and **C2** were fluorescent with little no emission for **1** and **2**. The lifetime determined for **C1** and **C2** in toluene were found to be 4.87 and 2.14 ns (Figure S1c).

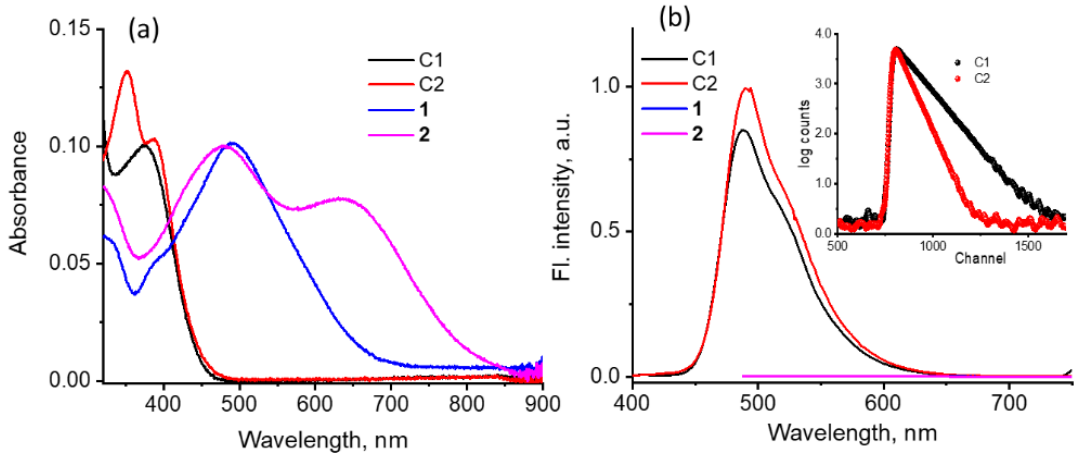

Figure 2. (a) Absorption and (b) fluoresence spectra of indicated compounds in benzonitrile. The compounds were excited at the visible peak maxima. Figure 2b inset shows fluorescence decay profiles of **C1** and **C2** in benzonitrile.

Since the location of the frontier orbitals in push-pull conjugates govern the extent of ground and excited state CT, compounds **1** and **2** were optimized at the CAM-B3LYP/6-31G(d,p) level,[36] and the frontier orbitals were generated in the gas phase, as shown in Figure 3. In the case of **1**, the HOMO was distributed all over the molecular system with higher coefficient on the central PTZ entity while the HOMO-1 was localized on the TPA-TCBD entities in a symmetrical fashion. Interestingly, the LUMO and LUMO+1 were symmetrically distributed over the TCBD entities with some coefficients on the PTZ ring nitrogen. These results are suggestive of central PTZ being push group and TCBDs to be pull groups in **1**. In contrast, in the case of **2**, asymmetric distribution of orbitals was observed. The HOMO was localized on the TPA-DCNQ entity while HOMO-1 was on the TPA-TCBD entity. The first LUMO was on the DCNQ entity while the LUMO+1 was on the TCBD entity. The location of LUMOs suggest that DCNQ being a better electron acceptor than TCBD. In the case of **2**, the CT would involve promoting electron from the TPA-DCNQ to DCNQ while in the case of **1**, CT transition would mainly involve promoting an electron from the central PTZ to TCBD. Incorporating the solvent term, nonpolar toluene or polar

acetonitrile, did not reveal significant changes in location or nature (symmetric versus asymmetric) of the frontier orbitals (see Figure S3 in SI)

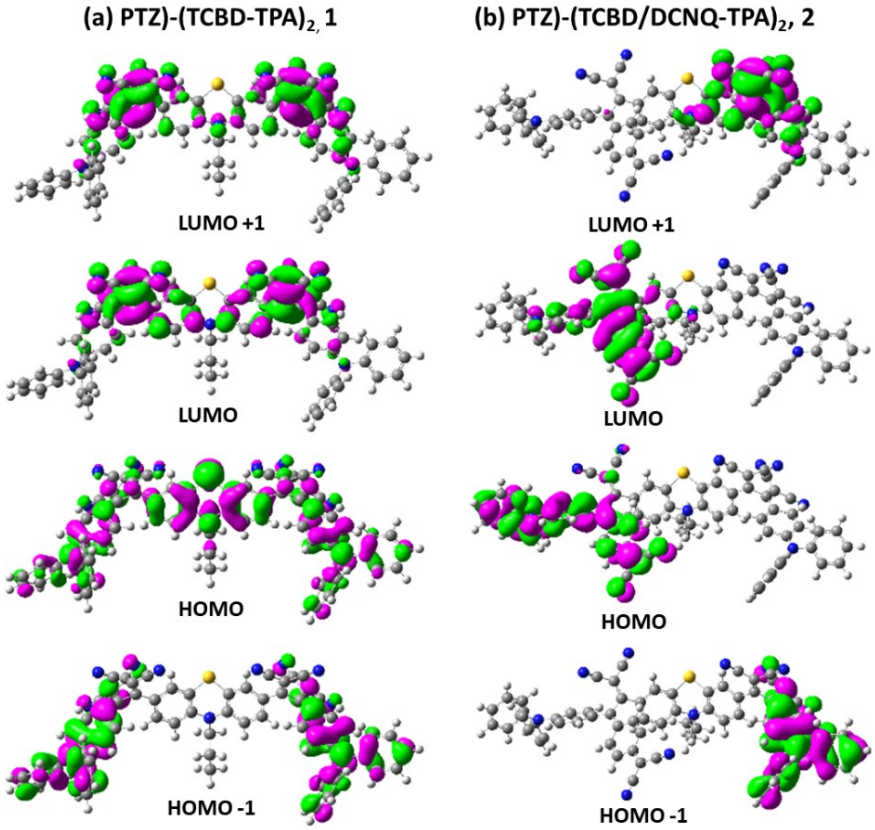

Figure 3. Frontier HOMO-1, HOMO, LUMO and LUMO+1 of (a) **1** and (b) **2** on CAM-B3LYP/6-31G(d,p) optimized structures.

In order to probe the effect of symmetrically positioned TCBD entities on the reduction potentials of **1**, that is, to seek existence of any electronic communication between the TCBD entities, and asymmetrically positioned TCBD and DCNQ in **2** as to their electron acceptor capability, cyclic (CV) and differential pulse voltammetry (DPV) experiments (see Figure 4) were performed. To summarize, PTZ oxidation in **C1** was located at 0.94 V vs. Ag/AgCl that was cathodically shifted to 0.87 V in **C2** due to the presence of two electron donating terminal TPA entities due to electronic inductive effects. Oxidation of TPA entities in **C2** occurred at 1.18 V. Presence of two TCBD entities in **1** resulted in anodic shift of PTZ oxidation to 1.32 V. Interestingly, the first reduction of TCBD in **1** revealed a split wave indicating the existence of intramolecular electron exchange, similar to that reported recently in central triphenylamine

derived, dimethylaminophenyl-tetracyanobutadiene donor-acceptor conjugates.[15] The split waves were located at -0.23 and -0.30 V (all reversible on CV time scale), that is, a 70 mV split was observed suggesting electron exchange between the two TCBD entities via the central PTZ entity. It may be pointed here that in multiple donor-TCBD bearing push-pull systems of this class, the central entity connecting to the donor-TCBD plays an important role promoting intramolecular electron exchange resulting in peak splitting. The central phenothiazine in the present system and triphenylamine from the recent example[14] promote such electron exchange as there is sufficient electronic communication between the central connecting unit and TCBD entities. However, when the central unit was a truxene scaffold having no intramolecular interactions with the TCBD entity,[11] such splitting of TCBD reduction wave was not observed, highlighting the significance of the central entity in establishing electronic communication between the two TCBD in this class of multi-modular systems. In the case of **2** having both TCBD and DCNQ electron acceptors, four reductions were observed (all reversible on CV time scale). The first two corresponding to the reductions of DCNQ were located at -0.07 and -0.16 V while the reductions of TCBD were located at -0.30 and -0.61 V. It is important to note that no split in either TCBD or DCNQ waves was observed in the case of **2**. The oxidation of PTZ was located at 1.23 V about 100 mV easier than that observed for **1**, although **2** had a better electron acceptor entity. This explains the pronounced red-shift in **2** (smaller HOMO-LUMO gap) compared to **1**. The easier oxidation could be attributed to extended π-conjugation offered by DCNQ ring compared to TCBD in **1** (see earlier discussed frontier orbitals).

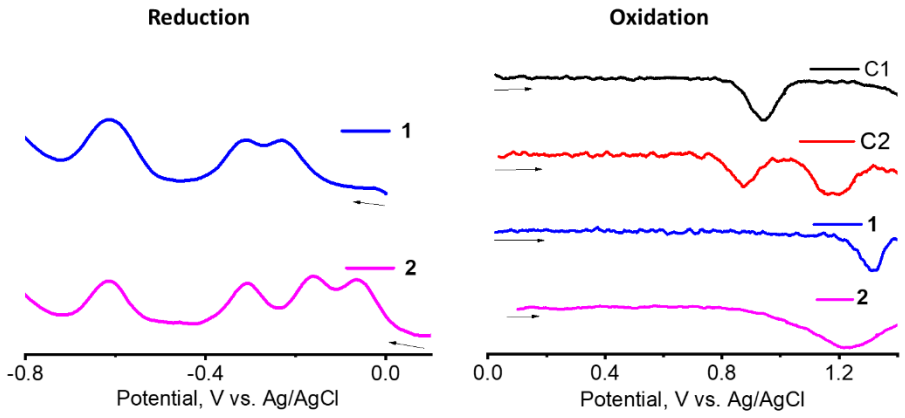

Figure 4. DPVs depicting reductions of **1** and **2**, and oxidations of **1** and **2** along with the controls in benzonitrile, 0.1 M (TBA)ClO_4. Both **C1** and **C2** had no reductions within the monitored potential window.

From the electrochemical, and excited singlet energy data, the free-energies of charge-separation (ΔG_{CS}) and charge recombination (ΔG_{CR}) were calculated using equations 1 and 2 by Rehm-Weller's approach.[37]

$$-\Delta G_{CS} = (\Delta E_{0,0}) - (-\Delta G_{CR}) \qquad (1)$$

$$-\Delta G_{CR} = (E_{ox} - E_{red}) + \Delta G_S \qquad (2)$$

where E_{ox} is the first one-electron oxidation potential of the donor, E_{red} is the first one-electron reduction potential of acceptor TCBD or DCNQ, $\Delta E_{0,0}$ is the excitation energy corresponding to the locally excited state, estimated from longer wavelength absorption peak edge. ΔG_S refers to the solvation energy, calculated by using the 'Dielectric Continuum Model' according to the following equation,

$$\Delta G_s = e^2 / 4\,\pi\,\varepsilon_o\,[(1/2R_+ + 1/2R_-)\,(1/\varepsilon_{s'}) - 1/R_{CC}\,\varepsilon_s] \qquad (3)$$

where R_+ and R_- refer to radii of the cation and anion species, respectively. R_{CC} is center-to-center distance between the donor and acceptor entities from computational modeling. The symbols ε_s ($\varepsilon_{s'} = \varepsilon_s - \varepsilon_R$), ε_0 and ε_R refer to dielectric constant of the solvent used for photophysical study, vacuum permittivity, and dielectric constant of the solvent used in electrochemical measurement, respectively. The calculated values are given in Table 1 below.

Table 1. Free-energy of different states of 1 and 2.

Compound	Solvent	$\Delta E_{0,0}$, eV	E_{CT}, eV	$-\Delta G_{CS}$, eV	$-\Delta G_{CR}$, eV
1	PhCN	1.91	1.80	0.65	1.26
	Toluene	1.91	1.80	-0.04	1.95
2	PhCN	1.69	1.61	0.64	1.05
	Toluene	1.69	1.61	-0.01	1.70

An energy level diagram was subsequently established to visualize the excited state events, as shown in Figure 5. Direct excitation of PTZ (shown as LE state in Figure 5) in **1** and **2**, would promote a CT state, viz., TPA-TCBD-PTZ$^{\delta+}$-TCBD$^{\delta-}$-TPA in the case of **1**, and TPA-TCBD-PTZ $^{\delta+}$-DCNQ$^{\delta-}$-TPA in the case of **2** from the corresponding initial singlet excited state. In the case of **1**, the partial negative charge could be on either of TCBD entities as suggested by the

location of almost degenerate LUMO and LUMO+1 in Figure 3a and split first reduction of TCBD. However, in the case of **2**, formation of TPA-TCBD-PTZ $^{\delta+}$-DCNQ$^{\delta-}$-TPA CT state is likely the case as revealed by the location of LUMO and facile reduction of DCNQ compared to TDCB. A TPA-TCBD$^{\delta-}$-PTZ $^{\delta+}$-DCNQ-TPA CT state in **2** is relatively a high-energy state. Subsequent formation of CS states, TPA-TCBD-PTZ$^{\bullet+}$-TCBD$^{\bullet-}$-TPA in the case of **1**, and TPA-TCBD-PTZ$^{\bullet+}$-DCNQ$^{\bullet-}$-TPA in the case of **2** is energetically feasible processes in benzonitrile. However, such CS in toluene is an uphill process in the case of both **1** and **2**. Finally, the CS state in benzonitrile and CT state in toluene could relax back to the ground state via the process of charge recombination (CR). It also important to note that due to geometry and energy considerations, both CT and CS processes could occur at a faster time scale. In order to witness the formation of such ultrafast photo-events, both conjugates were subjected to fs-TA studies in benzonitrile and toluene.

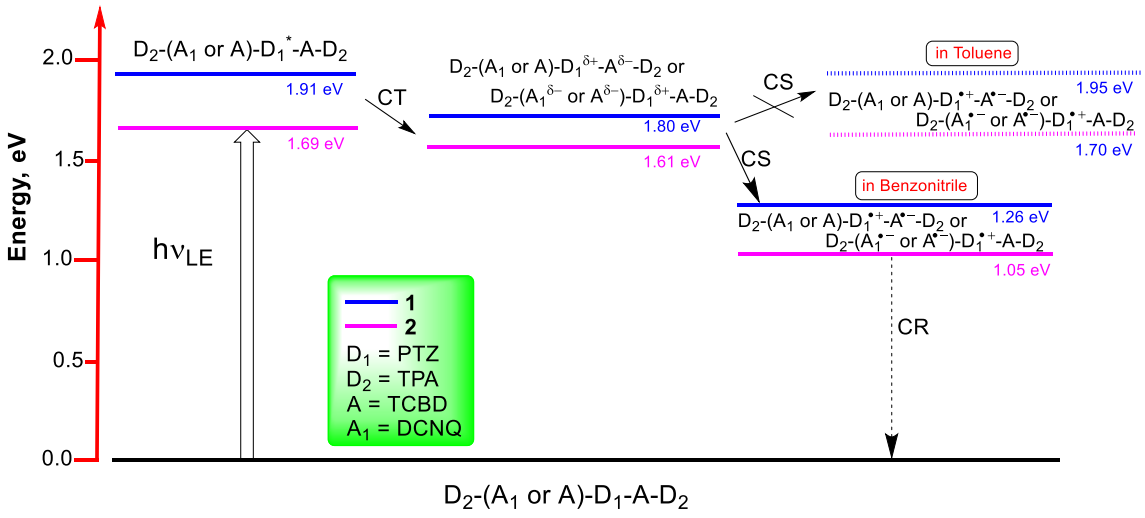

Figure 5. Energy level diagram revealing photo-evets leading to charge transfer (CT), charge separation and recombination in **1** (blue lines) and **2** (magenta lines) in benzonitrile (shown in solid lines) and toluene (shown in dashed lines).

Prior performing the transient spectral studies, to aid-in the spectral analysis of the charge separation products, spectroelectrochemical studies was performed on both **1** and **2** in benzonitrile. Here, spectrum of first oxidation and first reduction products of each compound was generated by applying appropriate voltage in a thin-layer spectroelectrochemical cell having transparent (Pt-gauze) working electrode in the light path. Spectral changes during oxidation and reduction of **1** and **2** are shown below. The **1**$^{\bullet+}$ was characterized by a new peak at 742 nm while spectrum of **1**$^{\bullet-}$

revealed diminished intensity of original peak with a less intense broad peak the 700 nm region (Figures 6a and b). The changes observed during the course of $\mathbf{2}^{\bullet+}$ formation were minimal, that is, only a slight overall increase in the absorption spectrum was observed. However, spectrum of $\mathbf{2}^{\bullet-}$ revealed a new broad peak in the 1100 nm range accompanied by diminished intensity of mainly the CT band (Figure 6d and e). Next, final spectrum of the radical cation and radical anion of a given conjugate was digitally added and subtracted with the spectrum of the initial neutral compound. The spectrum thus generated would largely represent the differential transient absorption spectrum expected for the electron transfer product, and would closely resemble to the species associated spectrum (SAS) of CS product generated from target analysis.[11] Figure 6c and f, respectively, show such spectrum derived for **1** and **2** covering the entire visible-near infrared region.

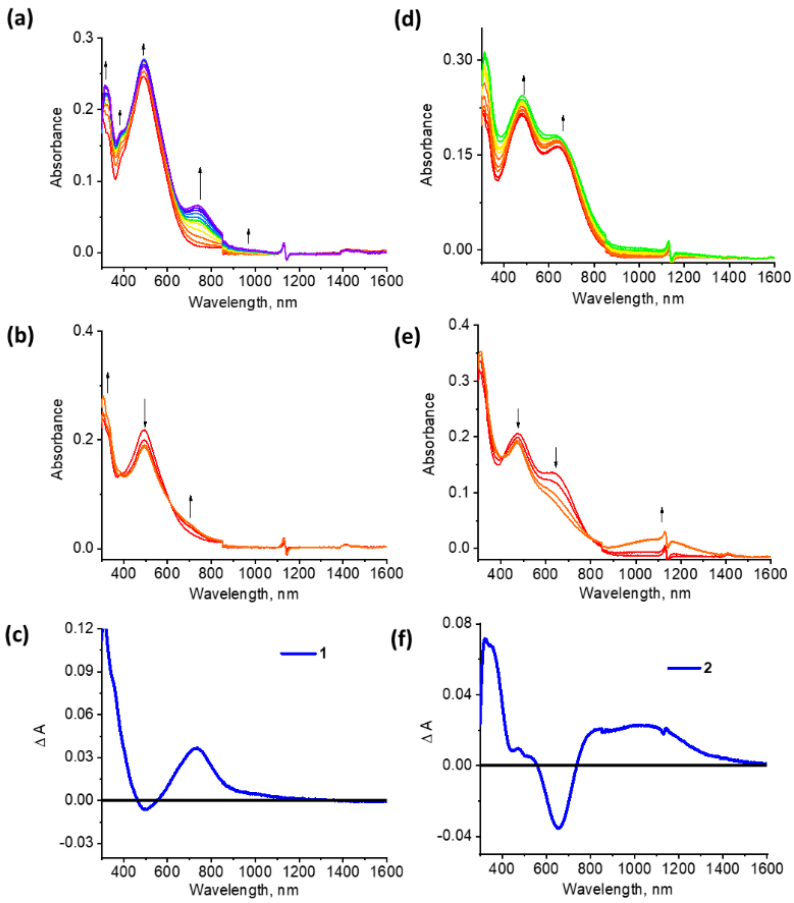

Figure 6. Spectral changes during first oxidation (a and d), during first reduction (b and e), and spectrum generated for the charge separated product (c and f, see text for details) of (a) **1** and (b) **2** in benzonitrile containing 0.2 M $TBAClO_4$.

Fs-TA spectra of the control compounds **C1** and **C2**, in benzonitrile and toluene, are shown in Figure S4. In the case of PTZ containing **C1**, the instantaneously formed singlet excited state (see spectrum at 2 ps delay time) revealed excited state absorptions (ESA) at 608 nm and a broad peak in the near-IR region having maxima at 1135 nm in benzonitrile (Figure S4a). A negative peak at 490 nm was also observed, and due to similarity of this peak with the earlier discussed fluorescence maxima (see Figure 2b), this signal has been attributed to stimulated emission (SE). These spectral features were largely retained for **C1** in nonpolar toluene (Figure S4b). ESA peaks at 613 and 1058 nm with a shoulder peak at 931 nm, and SE peak at 480 nm were observed. As shown in Figures S4 time profiles, the decay of ESA peaks were slow (applies also for recovery of SE peak). These results are consistent with ~ 5 ns fluorescence lifetime of **C1** in these solvents. As shown in Figures S4c and d for the case of **C2**, the transient spectra were appreciably different in both investigated solvents. In the visible region, two ESA peaks at ~610 and 720 nm were observed along with the near-IR peak in the ~1100 nm range, and SE emission peak in the 490 nm region. The second ESA peak could be due to ESA of appended TPA entities. Decay/recovery of ESA/SE peaks were comparatively fast (see Figures S4 for time profiles), consistent with the lifetime of **C2** of little over 2 ns.

Finally, fs-TA spectral properties of the push-pull systems **1** and **2** were investigated in both benzonitrile and toluene solvents. Figure7a(i) shows the transient spectra at the indicated delay times of **1** in benzonitrile, covering both visible and near-IR regions. The instantaneously formed singlet excited state, ^{1}**1*** revealed an ESA peak at 617 nm and a ground state bleach (GSB) peak ~500 nm where absorption maxima of **1** exists. Following this, within 5 ps, a new spectrum was formed with broad spectral peaks in the 700-750 nm expected for the CS state. Decay/recovery of ESA/GSB signals was rapid and by about 100 ps no residual signal could be detected. This suggests that the CS state directly leads to the ground state without populating any intermediate long-lived triplet excited states. It may be mentioned here that a strong bleach in the 1000 nm region that recovered on a faster time scale was observed in both push-pull systems, although the reasons are not clear, this could be due to stimulated emission of charge transfer emission or phosphorescence. Our attempts to seek either charge transfer emission in this spectral region or phosphorescence (at liquid nitrogen temperature in glass forming solvent) were not successful, implying very low quantum yields.

The transient spectral data was subjected to Glotaran target analysis[38-39] to capture spectrum of different species and associated population kinetic parameters. Both branched (S_1

state simultaneously forming CT and CS states), and sequential (S_1 → CT → CS) schemes were used, however, the best fit was obtained for the sequential model. As shown in Figure 7a(ii) and (iii), such analysis resulted in three SASs. The first spectrum with a time constant of 1.10 ps had features of the singlet excited state of ^{1}**1*** while the second spectrum with a time constant of 8.42

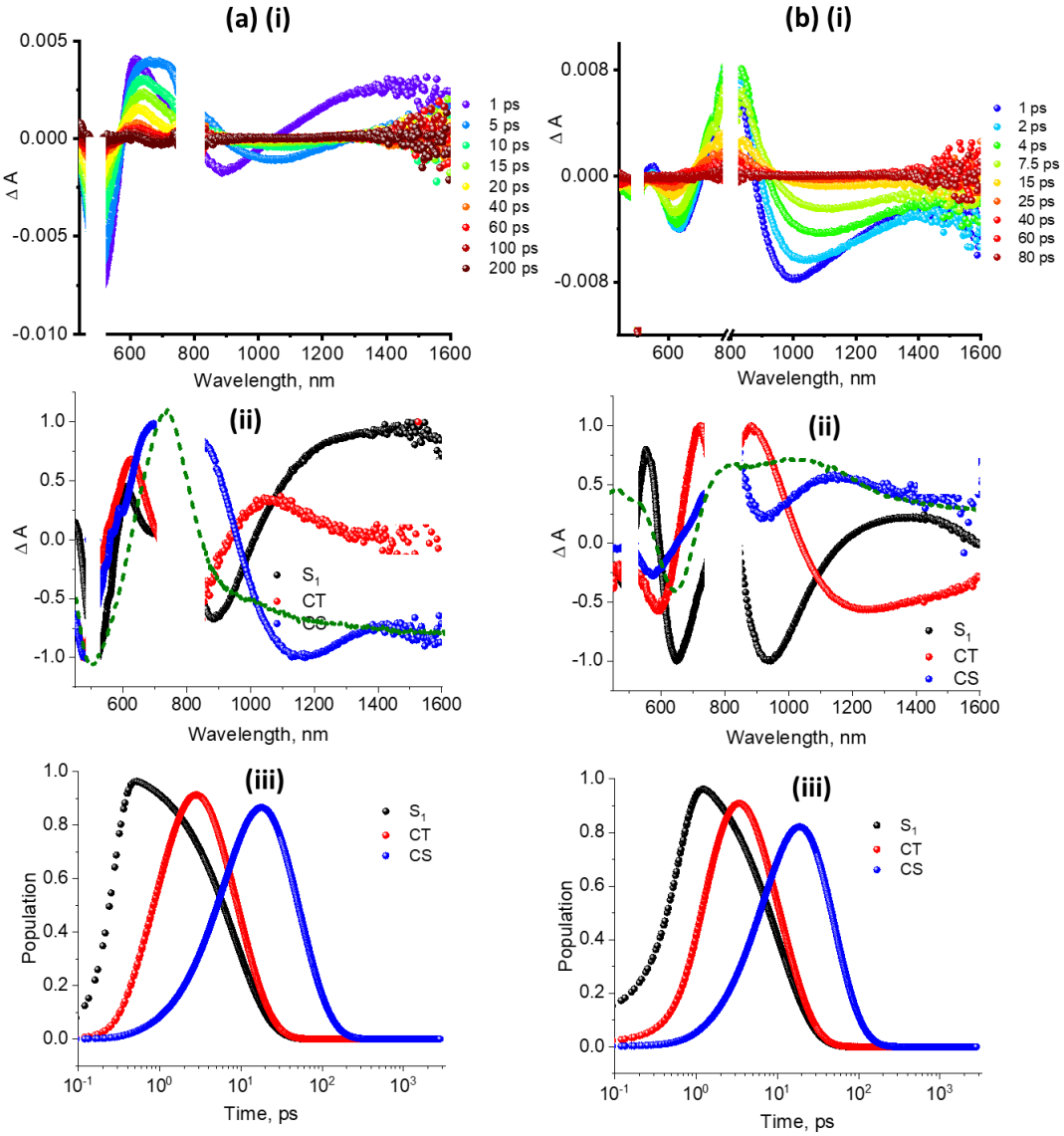

Figure 7. Fs-TA spectra at the indicated delay times of (a) **1** and (b) **2** in benzonitrile at the excitation wavelength of 500 nm. Species associate spectra (SAS), and population kinetics from target analysis, are shown beneath the transient spectra. The break in the 500 nm region is due to excitation laser pulse signal blocking and around 800 nm is due to detector change. The green dashed lines represent spectrum of charge separated state deduced from spectroelectrochemical studies.

ps had slight red-shifted ESA and blue-shifted GSA peak and this was attributed to the excited CT state. The final spectrum with a time constant of 43.91 ps largely resembled the spectrum of the CS state deduced earlier from spectroelectrochemical studies (see green dashed line), supporting CS in **1**. Here, the population time constants are average lifetime of a given state. It may be mentioned here that an exact match between the transient spectrum corresponding to CS state and that deduced from spectroelectrochemical studies would be difficult due to different experimental conditions of data collection (viz., spectroelectrochemical studies are done in the presence of supporting electrolyte while photochemistry in pure solvent), and residual contributions from ESA, GSB and SE signals to the spectrum associated with CS species from target analysis. However, a close resemblance between these two spectra would support formation of charge separated product.

The fs-TA spectra for **2**, excited at 500 nm corresponding to the LE state is shown in Figure 7b. The instantaneously formed ^{1}**2*** revealed ESA peaks at 550 and 740 nm and a GSB at 490 and 635 nm. The decay/recovery of the ESA/GSB peaks was associated with characteristic peak in the 760 nm range expected for the CS state (see spectrum at 4 ps in Figure 7b(i)). Target analysis of the transient spectra resulted in three SAS as shown in Figure 7b(ii). The first spectrum at 1.25 ps was attributed to ^{1}**2*** due to initial spectral resemblance of this state, the second spectrum at 6.73 ps with blue-shifted spectral features was associated with the charge transfer state and the final spectrum at 16.31 ps resembled closely to that of the charge separated state, deduced from spectroelectrochemical studies (compare blue trace in Figure 7(iii) and Figure 5(iv)), supporting CS in **2**. The population kinetics shown in Figure 7b(iii) suggested occurrence of faster photo-induced events in **2** than that in **1**.

Figures 8a and b show the fs-TA spectra at the indicated delay times of **1** and **2** in toluene at the excitation wavelength of 500 nm. The energy level diagram in Figure 5 predicted charge transfer but not change separation for both compounds in toluene. For the large part, the initial spectral features were close to that observed in benzonitrile, however, with subtle differences, especially in the region where CS features were expected. Further, the data was subjected to target analysis with two components fitting (S_1 and CT formation) whose spectra and populations kinetics are shown in Figure 8 below for each compound. For **1**, the S_1 and CT time constants were found to be 3.81 ps and 32.60 ps, while that for **2**, these values were 3.79 and 16.71 ps,

respectively. That is, the process of CT was faster in **2** than in **1**, similar to that observed earlier in benzonitrile. It is also important to note that due to close proximity of the donor and acceptor entities, both CT and CS processes in the studied push-pull systems were relatively fast.

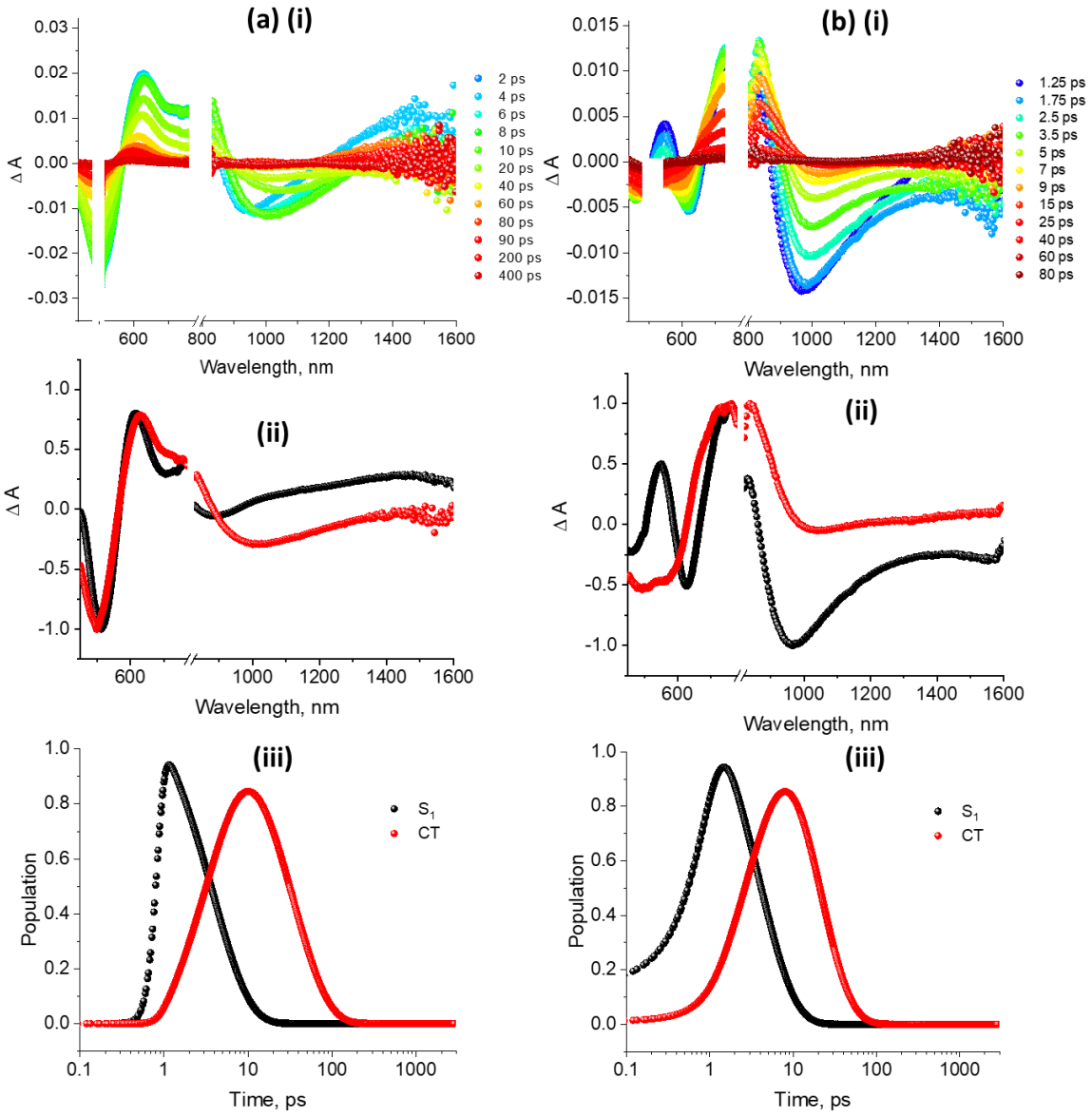

Figure 8. Fs-TA spectra at the indicated delay times of (a) **1** and (b) **2** in toluene at the excitation wavelength of 500 nm. Species associate spectra (SAS) and population kinetics from target analysis are shown beneath the transient spectra. The break in the 500 nm region is due to excitation laser pulse signal blocking and around 800 nm is due to detector change.

Table 2. Kinetic parameters deduced from Target analysis of transient absorption data for the studied push-pull donor-acceptor systems as a function of solvent polarity.[a]

Compound	λ_{ex}	solvent	τ_{S1}, ps	τ_{CT}, ps	τ_{CS}, ps
1	500	PhCN	1.10	8.42	43.91
2	500	PhCN	1.25	6.73	16.31
1	500	Toluene	3.81	32.60	--
2	500	Toluene	3.79	16.71	--

[a]-estimated error = $\pm$ 10%

Kinetic parameters arrived from the present study are summarized in Table 2. As pointed out earlier, due to close proximity of the donor and acceptor entities in this type of molecular systems,[11-15, 33-35] both CT and CS processes occur rapidly. Expectedly, increasing solvent polarity further accelerated these processes wherein formation of charge separated states was possible to observe in polar solvent. Between the TCBD and DCNQ acceptors, owing to better electron acceptor property of DCNQ, faster CT and CS events was possible to observe in DCNQ derived push-pull systems.

CONCLUSION

In summary, photoinduced processes occurring in push-pull systems comprised of a central phenothiazine (PTZ) derived symmetric **1** (PTZ-(TCBD-TPA)$_2$) and asymmetric, **2** (PTZ-(TCBD/DCNQ-TPA)$_2$) multi-modular conjugates is accomplished. Among the TCBD and DCNQ acceptors, facile reduction of DCNQ established it to be a better electron acceptor. Because of strong push-pull effects, CT was observed extending the absorption well into the near-IR region, especially for push-pull system **2** having DCNQ as an electron acceptor. The spectrum of CS product in **1** and **2** was possible to infer from manipulation of spectroelectrochemical data. Computational studies coupled with the established energy level diagram predicted occurrence of CS in these push-pull systems in polar benzonitrile but not in nonpolar toluene. Fs-TA studies along with global target analysis of transient spectral data, performed in both polar and nonpolar solvents, confirmed occurrence of such ultrafast photo-events in these push-pull systems in which the CS was much more efficient in unsymmetrical **2** having both TCBD and DCNQ acceptors.

The significance of number and strength of electron acceptor entities in multi-modular push-push systems is borne out from the present work.

ASSOCIATED CONTENT

Supporting Information. Additional spectral, computational and transient absorption data, compete citation details of ref. 36.

AUTHOR INFORMATION

Corresponding Authors

Francis D'Souza, E-mail: Francis.dsouza@unt.edu, ORCID.org/ 0000-0003-3815-8949

Rajneesh Misra, E-mail: rajneeshmisra@iiti.ac.in

Authors

Youngwoo Jang

Yogajivan Rout

Notes

The authors declare no competing financial interests.

ACKNOWLEDGMENT

Authors acknowledge the support from the DST, (DST/TMD/SERI /D05(C)), INSA (SP/YSP/139/2017/2293), SERB CRG/2018/ 000032 and CSIR 01(2934)/18/EMR–II, New Delhi Government of India, and US-National Science Foundation (2000988 to FD).

REFERENCES

(1) Wu, Z.; Liu, Y.; Yu, L.; Zhao, C.; Yang, D.; Qiao, X.; Chen, J.; Yang, C.; Kleemann, H.; Leo, K.; Ma, D. Strategic-Tuning of Radiative Excitons for Efficient and Stable Fluorescent White Organic Light-Emitting Diodes. *Nat. Commun*. **2019**, *10*, 2380. DOI:10.1038/s41467-019-10104-4.

(2) Kido, J.; Kimura, M.; Nagai, K. Multilayer White Light-emitting Organic Electroluminescent Device. *Science*, **1995**, *267*, 1332–1334. DOI:10.1126/science.267.5202.1332

(3) Ye, J.; Zheng, C.-J.; Ou, X.-M.; Zhang, X.-H.; Fung, M.-K.; Lee, C.-S. Management of Singlet and Triplet Excitons in a Single Emission Layer: A Simple Approach for a High-Efficiency Fluorescence/Phosphorescence Hybrid White Organic Light-Emitting Device. *Adv. Mater*. **2012**, *24*, 3410–3414, DOI:10.1002/adma.201201124.

(4) Babgi, B.; Rigamonti, L.; Cifuentes, M. P.; Corkery, T. C.; Randles, M. D.; Schwich, T.; Petrie, S.; Stranger, R.; Teshome, A.; Asselberghs, I. et. al., Length-Dependent Convergence and Saturation Behavior of Electrochemical, Linear Optical, Quadratic Nonlinear Optical, and Cubic Nonlinear Optical Properties of Dipolar Alkynylruthenium Complexes with Oligo(Phenyleneethynylene) Bridges. *J. Am. Chem. Soc*. **2009**, *131*, 10293–10307, DOI:10.1021/ja902793z.

(5) Yang, Z.; Jazbinsek, M.; Ruiz, B.; Aravazhi, S.; Gramlich, V.; Günter, P. Molecular Engineering of Stilbazolium Derivatives for Second-Order Nonlinear Optics. *Chem. Mater.* **2007**, *19*, 3512–3518, DOI:10.1021/cm070764e.

(6) Chen, J. J.; Conron, S. M.; Erwin, P.; Dimitriou, M.; McAlahney, K.; Thompson, M. E. High-Efficiency BODIPY-Based Organic Photovoltaics. *ACS Appl. Mater. Interfaces* **2015**, *7*, 662–669, DOI:10.1021/am506874k.

(7) Peng, J.; Chen, Y.; Wu, X.; Zhang, Q.; Kan, B.; Chen, X.; Chen, Y.; Huang, J.; Liang, Z. Correlating Molecular Structures with Transport Dynamics in High-Efficiency Small-Molecule Organic Photovoltaics. *ACS Appl. Mater. Interfaces* **2015**, *7*, 13137–13141, DOI:10.1021/acsami.5b03073.

(8) Rout, Y.; Jang, Y.; Gobeze, H. B.; Misra, R.; D'Souza, F. Conversion of Large-Bandgap Triphenylamine–Benzothiadiazole to Low-Bandgap, Wide-Band Capturing Donor–Acceptor Systems by Tetracyanobutadiene and/or Dicyanoquinodimethane Insertion for Ultrafast Charge Separation. *J. Phys. Chem. C* **2019**, *123*, 23382–23389, DOI:10.1021/acs.jpcc.9b06632.

(9) Gautam, P.; Misra, R.; Siddiqui, S. A.; Sharma, G. D. Unsymmetrical Donor–Acceptor–Acceptor−π–Donor Type Benzothiadiazole-Based Small Molecule for a Solution Processed Bulk Heterojunction Organic Solar Cell. *ACS Appl. Mater. Interfaces* **2015**, *7*, 10283–10292, DOI:10.1021/acsami.5b02250.

(10) Carlotti, B.; Poddar, M.; Elisei, F.; Spalletti, A.; Misra, R. Energy-Transfer and Charge-Transfer Dynamics in Highly Fluorescent Naphthalimide–BODIPY Dyads: Effect of BODIPY Orientation. *J. Phys. Chem. C* **2019**, *123*, 24362–24374, DOI:10.1021/acs.jpcc.9b05851.

(11) Sharma, R.; Thomas, M. B.; Misra, R.; D'Souza, F. Strong Ground- and Excited-State Charge Transfer in C3-Symmetric Truxene-Derived Phenothiazine-Tetracyanobutadine and Expanded Conjugates. *Angew. Chem. Int. Ed*. **2019**, *58*, 4350–4355, DOI:10.1002/anie.201814388.

(12) Poddar, M.; Jang, Y.; Misra, R.; D'Souza, F. Excited-State Electron Transfer in 1,1,4,4-Tetracyanobuta-1,3-Diene (TCBD)- and Cyclohexa-2,5-Diene-1,4-Diylidene-Expanded TCBD-Substituted BODIPY-Phenothiazine Donor–Acceptor Conjugates. *Chem. Eur. J.* **2020**, *26*, 6869–6878, DOI:10.1002/chem.202000346.

(13) Pinjari, D.; Alsaleh, A. Z.; Patil, Y.; Misra, R.; D'Souza, F. Interfacing High-Energy Charge-Transfer States to a Near-IR Sensitizer for Efficient Electron Transfer upon Near-IR Irradiation, *Angew. Chem. Int. Ed*. **2020**, *59*, 23697-23705. doi.org/10.1002/anie.202013036

(14) Shoji, T.; Ito, S.; Toyota, K.; Yasunami, M.; Morita, N. Synthesis, Properties and Redox Behavior of Mono-, Bis, and Tris[1,1,4,4,-tetracyano-2-(1-azulenyl)-3-butadienyl] Chromophores Binding with Benzene and Thiophene Cores, *Chem. Eur. J*. **2008**, *14*, 8398-8408. DOI: 10.1002/chem.200701981

(15) Yadav, I. S.; Alsaleh, A. Z.; Misra, R.; D'Souza, F. Charge Stabilization via Electron Exchange: Excited Charge Separation in Symmetric, Central Triphenylamine Derived, Dimethylaminophenyl-Tetracyanobutadiene Donor-Acceptor Conjugates, *Chem. Sci*., **2020**, *12*, 1109-1120. DOI: 10.1039/d0sc04648e

(16) Leliege, A.; Blancharde, P.; Rousseau, T.; Roncali, J. Triphenylamine/ Tetracyanobutadiene-Based D-A-D p-Conjugated Systems as Molecular Donors for Organic Solar Cells, *Org. Lett*. **2011**, *13*, 3098-3101. https://doi.org/10.1021/ol201002j

(17) Blanco, G. D.; Hiltunen, A. J.; Lim, G. N.; KC, C. B.; Kaunisto, K. M.; Vuorinen, T. K.; Nesterov, V. N.; Lemmetyinen, H. J.; D'Souza, F. Syntheses, Charge Separation, and Inverted Bulk Heterojunction Solar Cell Application of Phenothiazine–Fullerene Dyads. *ACS Appl. Mater. Interfaces* **2016**, *8*, 8481–8490. DOI:10.1021/acsami.6b00561.

(18) Hart, A. S.; K. C., C. B.; Subbaiyan, N. K.; Karr, P. A.; D'Souza, F. Phenothiazine-Sensitized Organic Solar Cells: Effect of Dye Anchor Group Positioning on the Cell Performance. *ACS Appl. Mater. Interfaces* **2012**, *4*, 5813–5820. DOI:10.1021/am3014407.

(19) Salunke, J.; Guo, X.; Lin, Z.; Vale, J. R.; Candeias, N. R.; Nyman, M.; Dahlström, S.; Österbacka, R.; Priimagi, A.; Chang, J. et. al. Phenothiazine-Based Hole-Transporting Materials

toward Eco-Friendly Perovskite Solar Cells. *ACS Appl. Energy Mater*. **2019**, *2*, 3021–3027, DOI:10.1021/acsaem.9b00408.

(20) Barkschat, C. S.; Stoycheva, S.; Himmelhaus, M.; Müller, T. J. J. Synthesis, Electronic Properties, and Self-Assembly on Au{111} of Thiolated Phenylethynyl Phenothiazines. *Chem. Mater*. **2010**, *22*, 52–63, DOI:10.1021/cm901514t.

(21) Meyer, T.; Ogermann, D.; Pankrath, A.; Kleinermanns, K.; Müller, T. J. J. Phenothiazinyl Rhodanylidene Merocyanines for Dye-Sensitized Solar Cells. *J. Org. Chem*. **2012**, *77*, 3704–3715. DOI:10.1021/jo202608w.

(22) Xu, B.; Mu, Y.; Mao, Z.; Xie, Z.; Wu, H.; Zhang, Y.; Jin, C.; Chi, Z.; Liu, S.; Xu, J. et. al. Achieving Remarkable Mechanochromism and White-Light Emission with Thermally Activated Delayed Fluorescence through the Molecular Heredity Principle. *Chem. Sci.* **2016**, *7*, 2201–2206, DOI:10.1039/c5sc04155d.

(23) Ko, K.-J.; Lee, H. B.; Kim, H. M.; Lee, G. J.; Shin, S.-R.; Kumar, N.; Song, Y. M.; Kang, J.-W. High-Performance, Color-Tunable Fiber Shaped Organic Light-Emitting Diodes. *Nanoscale* **2018**, *10*, 16184–16192, DOI:10.1039/c8nr05120h.

(24) Jou, J.-H.; Sahoo, S.; Dubey, D. K.; Yadav, R. A. K.; Swayamprabha, S. S.; Chavhan, S. D. Molecule-Based Monochromatic and Polychromatic OLEDs with Wet-Process Feasibility. *J. Mater. Chem. C* **2018**, *6*, 11492–11518, DOI:10.1039/c8tc04203a.

(25) Chen, X.; Yang, Z.; Xie, Z.; Zhao, J.; Yang, Z.; Zhang, Y.; Aldred, M. P.; Chi, Z. An Efficient Yellow Thermally Activated Delayed Fluorescence Emitter with Universal Applications in Both Doped and Non-Doped Organic Light-Emitting Diodes. *Mater. Chem. Front*. **2018**, *2*, 1017–1023, DOI:10.1039/c8qm00064f.

(26) Yang, Z.; Mao, Z.; Xu, C.; Chen, X.; Zhao, J.; Yang, Z.; Zhang, Y.; Wu, W.; Jiao, S.; Liu, Y. et. al. Sterically Hindered Asymmetric D–A–D′ Thermally Activated Delayed Fluorescence Emitter for Highly Efficient Non-Doped Organic Light-Emitting Diodes. *Chem. Sci*. **2019**, *10*, 8129–8134, DOI:10.1039/c9sc01686d.

(27) Tanaka, H.; Shizu, K.; Nakanotani, H.; Adachi, C. Twisted Intramolecular Charge Transfer State for Long-Wavelength Thermally Activated Delayed Fluorescence. *Chem. Mater*. **2013**, *25*, 3766–3771, DOI:10.1021/cm402428a.

(28) Obondi, C. O.; Lim, G. N.; Karr, P. A.; Nesterov, V. N.; D'Souza, F. Photoinduced Charge Separation in Wide-Band Capturing, Multi-Modular Bis(Donor Styryl)BODIPY–Fullerene Systems. *Phys. Chem. Chem. Phys*. **2016**, *18*, 18187–18200, DOI:10.1039/c6cp03479a.

(29) Scattergood, P. A.; Delor, M.; Sazanovich, I. V; Bouganov, O. V; Tikhomirov, S. A.; Stasheuski, A. S.; Parker, A. W.; Greetham, G. M.; Towrie, M.; Davies, E. S., et. al., Electron Transfer Dynamics and Excited State Branching in a Charge-Transfer Platinum(II) Donor–Bridge-Acceptor Assembly. *Dalton Trans*. **2014**, *43*, 17677–17693, DOI:10.1039/c4dt01682c.

(30) Rout, Y.; Gautam, P.; Misra, R. Unsymmetrical and Symmetrical Push–Pull Phenothiazines. *J. Org. Chem*. **2017**, *82*, 6840–6845, DOI:10.1021/acs.joc.7b00991.

(31) Bruce, M. I.; Rodgers, J. R.; Snow, M. R.; Swincer, A. G. Cyclopentadienyl-Ruthenium and -Osmium Chemistry. Cleavage of Tetracyanoethylene under Mild Conditions: X-Ray Crystal Structures of $[Ru\{\eta^3\text{-}C(CN)_2CPhC{=}C(CN)_2\}(PPh_3)(\eta\text{-}C_5H_5)]$ and $[Ru\{C[{=}C(CN)_2]CPh{=}C(CN)_2\}\text{-}(CNBu^t)(PPh_3)(\eta\text{-}C_5H_5)]$. *J. Chem. Soc. Chem. Commun*. **1981**, No. 6, 271–272, DOI:10.1039/c39810000271.

(32) Kivala, M.; Boudon, C.; Gisselbrecht, J.-P.; Seiler, P.; Gross, M.; Diederich, F. A Novel Reaction of 7,7,8,8-Tetracyanoquinodimethane (TCNQ): Charge-Transfer Chromophores by [2 + 2] Cycloaddition with Alkynes. *Chem. Commun*. **2007**, No. 45, 4731–4733, DOI:10.1039/b713683h.

(33) Winterfeld, K. A.; Lavarda, G.; Guilleme, J.; Sekita, M.; Guldi, D. M.; Torres, T.; Bottari, Subphthalocyanine Axially Substituted with a Tetracyanobuta-1,3-diene-Aniline Moiety: Synthesis, Structure, and Physicochemical Properties. *J. Am. Chem. Soc.* **2017**, *139*, 5520-5529. DOI: 10.1021/jacs.7b01460.

(34) Sekita, M.; Ballesteros, B.; Diederich, F.; Guldi, D. M.; Bottari, G.; Torres, T. Intense Ground-State Charge-Transfer Interactions in Low-Bandgap Panchromatic Phthalocyanine-Tetracyanobuta-1,3-diene Conjugates, *Angew. Chem. Int. Ed*. **2016**, *55*, 5560-5564. DOI: 10.1002/anie.201601258.

(35) Poddar, M.; Cesaretti, A.; Ferraguzzi, E.; Carlotti, B.; Misra, R. Singlet and Triplet Excited-State Dynamics of 3,7-Bis(arylethynyl)phenothiazines: Intramolecular Charge Transfer and Reverse Intersystem Crossing, *J. Phys. Chem. C* **2020**, *124*, 17864-17878. https://dx.doi.org/10.1021/acs.jpcc.0c01786

(36) Frisch, M. J.; Trucks, G. W.; Schlegel, H. B.; Scuseria, G. E.; Robb, M. A.; Cheeseman, J. R.; Scalmani, G.; Barone, V.; Mennucci, B.; Petersson, G. A. et. al., *Gaussian 09*., revision A.02, Gaussian, Inc., Wallingford, CT, 2009.

(37) Rehm, D.; Weller, A. Kinetics of Fluorescence Quenching by Electron and Hydrogen-Atom Transfer. *Isr. J. Chem*. **1970**, *8*, 259−271. https://doi.org/10.1002/ijch.197000029

(38) Snellenburg, J. J.; Laptenok, S. P.; Seger, R.; Mullen, K. M.; van Stokkum, I. H. M. Glotaran: A Java-Based Graphical User Interface for the R Package TIMP. *J. Stat. Softw*. **2012**, *49*, 1–22, DOI:10.18637/jss.v049.i03.

(39) http://glotaran.org/.

TOC Graphic

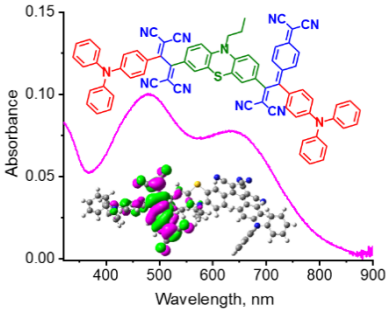
0.15
0.10
0.05
0.00
Absorbance
400
500
600
700
800
900
Wavelength, nm
NC
CN
N
S